MIMO Channel for Modal Multiplexing in Highly Overmoded Optical Waveguides

Daniel Lenz[1], Boris Rankov[2], Daniel Erni[1], Werner Bächtold[1] and Armin Wittneben[2]

[1]Laboratory for Electromagnetic Fields and Microwave Electronics, [2]Communication Technology Laboratory
Swiss Federal Institute of Technology (ETH) Zürich, CH-8092 Zürich, Switzerland
Email: {dlenz, erni, baechtold}@ifh.ee.ethz.ch, {rankov, wittneben}@nari.ee.ethz.ch

***Abstract*— In order to meet the increasing demand for data rate in modern multi-processor systems optical transmission has become an important technology. Due to cost reasons only highly multimodal waveguides come into question for mass-producible board level interconnects. We present the idea of an optical multiple-input multiple-output (MIMO) channel by having more than one data source at the channel input and a multi-segmented photodetector at the channel output. We develop channel models for the optical MIMO channel and show that orthogonality between modes in a highly multimodal waveguide can be exploited to submit independent data streams over different mode groups (*modal multiplexing*). Our performance results in terms of bit error rates show that the MIMO scheme outperforms the SISO scheme when the data rate is the same. Hence, optical MIMO schemes allows either to increase the data rate by keeping the amount of intersymbol interference (ISI) constant or to reduce the ISI by keeping the data rate constant.**

I. Introduction

Optical transmission has become the future data communication technology on multi-layered Printed Circuit Boards (PCBs) to meet the increasing demand for communication bandwidth of modern multiprocessor systems [1], [2]. For mass-producible board level interconnects only multimode waveguides are applicable due to the inappropriateness of clean room technologies and the relaxed tolerance requirements compared to singlemode technology. Such waveguides have very large cross sectional dimensions (100×100 μm) and are guiding up to several thousand modes. The drawback of multimode waveguides is the mode dispersion caused by the different propagation delays of the modes. Optical communication systems using multimode waveguides are thus rather dispersion limited than noise limited and require the application of equalizers.

Argon et al. [3] proposed recently a multi-segmented detector to obtain spatial diversity in a single-input multiple-output (SIMO) multimode fiber communication channel. In this work we extend the concept of [3] and present the idea of an optical multiple-input multiple-output (MIMO) channel by having more than one laser source at the channel input and a multi-segmented detector at the output. MIMO communication systems are well known from the wireless communication literature where antenna arrays at the transmit and receive side introduce additional degrees of freedom (spatial dimension) into a wireless communication system [4]. There are two basic space-time processing methods which make use of these degrees of freedom in MIMO systems, namely *space-time coding* to improve link reliability and *spatial multiplexing* to increase spectral efficiency. With spatial multiplexing it is possible to enhance the data rate without additional cost of bandwidth or power by transmitting simultaneously over spatial subchannels [4].

We introduce here the concept of *modal multiplexing* where we exploit the orthogonality between modes in a highly multimodal waveguide to submit independent data streams over different mode groups. This may help to overcome the limitation imposed by the intersymbol interference (ISI) caused by signal dispersion since the symbol duration may be relaxed without reducing the data rate.

The remainder of the paper is organized as follows: Section II describes the optical communication system and the physical models that are applied in order to obtain the parameters for the channel model that is deduced in Section III. A simple receiver scheme for SISO and MIMO transmission and performance results are demonstrated in Section IV.

II. System Description and Physical Models

The investigated optical communication system consists of a Vertical-Cavity Surface-Emitting Laser (VCSEL) source which is butt-coupled to a rectangular optical waveguide embedded in a PCB (Figure 1). For the sake of simplicity we assume a straight, perfect waveguide, i.e., no bends and no surface roughness are taken into account. Since the waveguides are embedded in a PCB, the length of the waveguide shall not exceed a few meters. At the receiver side a photodetector array is assumed. The idea is to take the optical communication system as a MIMO system. Therefore multiple inputs are required as well. Among the many possibilities of realizing multiple inputs we propose a segmented VCSEL contact geometry [5] to realize two sources within one VCSEL. Applying the proposed asymmetric drive scheme based on individually addressable segmented VCSEL contacts, a preferential excitation of modes with given azimuthal distribution is possible [5]. Hence, in the following sections we assume the VCSEL to excite two dominant independent controllable modes, namely the LP_{11}^{c} and the LP_{11}^{s} mode [6].

A rigorous treatment of the entire communication system, i.e., laser, far field transformation, mode coupling and mode propagation through the oversized waveguide, is not possible.

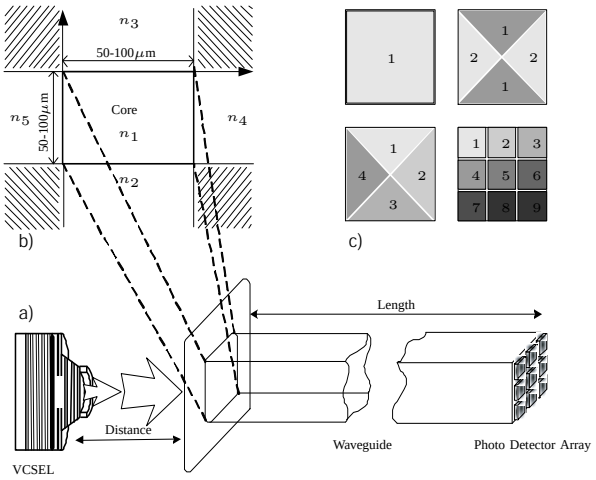

Fig. 1. (a) System Overview with VCSEL, waveguide and photodetector array. (b) Schematic of the five separable dielectric regions of a rectangular dielectric waveguide model. (c) Geometry of possible detector arrays.

In order to establish a tractable channel model it is necessary to apply approximative physical models which are briefly discussed below.

The optical field distribution at the VCSEL facet is simulated by using VISTAS, a comprehensive system-oriented spatio-temporal 2D VCSEL model [6]. To establish a reasonable channel model one needs to know the amount of power in each individual waveguide mode excited by the VCSEL. The power coupling coefficients are obtained by calculating the overlap integral [7] between each mode of the waveguide and the far field of each VCSEL mode at the end face of the waveguide input. This field is calculated by applying scalar diffraction theory [8]. Furthermore, all modes of the rectangular waveguide shown in Figure 1b) must be calculated. An exact analytical treatment for waveguides with rectangular cross-sections is not possible. We apply the approximation proposed by Marcatili [9] which neglects the fields in the shaded regions. Finally, the amount of power received by every individual photodetector is calculated using the Poynting vector [10].

III. Channel Model

We now deduce the channel model depicted in Figure 2 for the optical MIMO communication system. Note that baseband notation is used for the signals within this section. The input signals $\mathbf{s}(t) = [s_1(t), s_2(t), ..., s_m(t)]^{\mathrm{T}} = p(t) \cdot \mathbf{a}$ represent the field amplitude of the individual controllable laser modes, where $p(t)$ is the pulse form and $\mathbf{a} = [a_1, a_2, ..., a_m]^{\mathrm{T}}$ is the data vector with elements $a_i \in \{0, 1\}$. On the other hand, the vector $\mathbf{r}(t) = [r_1(t), r_2(t), ..., r_n(t)]^{\mathrm{T}}$ stands for the power that is received by the detector array. We assume m independent input signals, n spatially separated photodetectors at the receiver side and a waveguide that may guide k bound modes [9]. The matrix $\eta_{(\mathrm{in})}$ contains the input coupling coefficients that describe the coupling process from the laser modes to the waveguide modes. Knowledge about the individual modal amplitudes is important since we want

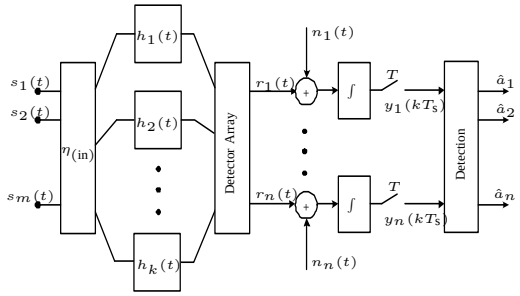

Fig. 2. Optical MIMO channel model and simple receiver, the noise is due to thermal noise in the electronics.

to understand, how the different input signals spread among the different modes of the waveguide. The modal amplitudes $\mathbf{\Phi}_{(\mathrm{in})}(t) = [\Phi_1^{(\mathrm{in})}(t), \Phi_2^{(\mathrm{in})}(t), ..., \Phi_k^{(\mathrm{in})}(t)]^{\mathrm{T}}$ at the waveguide input may be written as

$$\mathbf{\Phi}_{(\mathrm{in})}(t) = \eta_{(\mathrm{in})}\mathbf{s}(t), \tag{1}$$

where $\Phi_i^{(\mathrm{in})}(t)$ represents the modal amplitude of the ith bound mode. As aforementioned a perfect straight waveguide is assumed and therefore only negligible coupling between the guided modes takes place. Every mode has its individual phase velocity and thus its individual impulse response $h_i(t) = \exp(-j\beta_0^{(i)}L)\delta(t - \tau_i)$, where $\beta_0^{(i)}$ is the first order approximation of the phase parameter $\beta_0^{(i)} = \beta(\omega_0)$, $\tau_i = L\frac{\mathrm{d}\beta(\omega)}{\mathrm{d}\omega}$ is the group delay time for the ith mode and L is the waveguide length. For the sake of simplicity, we do not consider intra-mode dispersion in our present treatment. With the impulse response vector $\mathbf{h}(t) = [h_1(t), h_2(t), ..., h_k(t)]^{\mathrm{T}}$ the modal amplitudes at the far end of the waveguide can be expressed as

$$\mathbf{\Phi}_{(\mathrm{out})}(t) = \mathbf{h}(t) \otimes \mathbf{\Phi}_{(\mathrm{in})}(t), \tag{2}$$

where $\otimes$ denotes the element wise convolution. In order to calculate the power received by the ith photodetector it is necessary to integrate the Poynting vector $\mathbf{S}$ of the field distribution at the end of the waveguide over the area A_i of the ith photodetector, i.e.,

$$r_i = \frac{1}{2}\,\mathrm{Re}\left\{\int_{A_i} \mathbf{S} \cdot \mathbf{e}_z \; \mathrm{d}A_i\right\} \tag{3}$$

where $\mathbf{e}_z$ is the unit vector perpendicular to the area of the photodetector. Note that the calculations are based on the weak guidance approximation [10], i.e., only transversal field components are considered. After some algebraic manipulation of (3) we find [11]

$$r_i(t) \simeq \sum_{m=1}^{k}\sum_{l=1}^{k} R_{m,l}^{(i)} q_m(t) q_l^*(t) \eta_{(\mathrm{in})}^{(m)} \mathbf{a} \left(\eta_{(\mathrm{in})}^{(l)}\mathbf{a}\right)^*, \tag{4}$$

where $q_i(t) = h_i(t) * p(t)$ and $*$ denotes convolution as well as conjugate transpose. The coefficient

$$R_{m,l}^{(i)} = \int_{A_i} \Psi_m(x,y)\Psi_l^*(x,y) \; \mathrm{d}A_i \tag{5}$$

expresses the correlation between the individual modes over the area A_i of photodetector i. The function $\Psi_m(x,y)$ is the transversal distribution of the mth modal field [9]. Equation (4) is based on the assumption that the incident field is linearly polarized. Assuming different polarized input signals will lead to a slightly different expression. Regarding the interesting case with two different polarized input signals, e.g., the LP_{11}^{c} and LP_{11}^{s} mode, yields [11]

$$r_i(t) \simeq \left\{ \begin{array}{l} a_1 \underbrace{\sum_m \sum_l R_{mi,l}^{(i,x)} q_x^{(m)}(t) q_x^{*(l)}(t) \eta_x^{(m)} \eta_x^{*(l)}}_{h_{i1(t)}} \\ +a_2 \underbrace{\sum_m \sum_l R_{m,l}^{(i,y)} q_y^{(m)}(t) q_y^{*(l)} \eta_m^{(y)}(t) \eta_m^{*(l)}}_{h_{i2(t)}} \end{array} \right\}$$
$$= \mathbf{H}^{(i)}\mathbf{a} \;\text{ with }\; \mathbf{a} = [a_1\ a_2]\,, \qquad (6)$$

where x and y are the polarization indices and $\mathbf{H}^{(i)}$ is the ith row vector $[h_{i1}(t), h_{i2}(t)]$ of the matrix $\mathbf{H}$. With that, a manageable expression for the power at the photodetector array can be given by $\mathbf{r} \simeq \mathbf{H}\mathbf{a}$.

Channel Model Results. We simulated the optical MIMO channel model described by equation (6) with a 50×50 μm waveguide having a refractive index $n_{\mathrm{co}} = 1.5$ for the core and $n_{\mathrm{cl}} = 1.485$ for the cladding, respectively. The VCSEL is assumed to lase at $\lambda = 850$ nm. The approximative physical models described in Section II are used to determine the parameters, i.e., coupling coefficients $\eta_{(\mathrm{in})}$, impulse response vector $\mathbf{h}(t)$ and the correlation coefficients $R_{m,l}^{(i)}$. Figure 3 shows the far fields of the two laser modes LP_{11}^{c} and LP_{11}^{s} that couple into the waveguide. Figure 3c) shows the distribution of power versus mode number assuming an illumination by the LP_{11}^{s} mode whereas Figure 3d) assumes a LP_{11}^{c} source mode. The mode number has been chosen such that

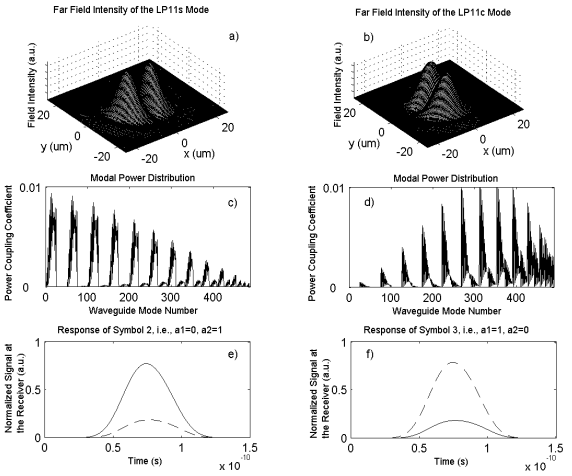

Fig. 3. Far field and modal power distribution: (a) Far field intensity of the LP_{11}^{s}. (b) Far field intensity of the LP_{11}^{c}. (c) Modal power distribution of the x-polarized modes. (d) Modal power distribution of the y-polarized modes. Signal at the different detectors after 1m waveguide caused by the input symbol: (e) $a_1 = 0$, $a_2 = 1$ (f) $a_1 = 1$, $a_2 = 0$

the transversal distributions $\Psi_m(x,y)$ of different polarized modes with the same mode number coincide in order to point out the spatial overlap of the modal fields excited by the different polarized sources. It becomes apparent, that the two sources excite different transversal distributions as long as the mode number is low. Higher order modal distributions are excited by both source modes leading to channel cross-talk as it can be seen in Figures 3e) and 3f) which shows the power received by a two element photodetector array configured as depicted in Figure 1c).

The pulse form $p(t)$ is assumed to be a normalized Gaussian with $\sigma = \frac{T_{\mathrm{s}}}{4}$ [12]. The symbol duration is $T_{\mathrm{s}} = 100$ ps and the length of the waveguide is one meter. The cross-talk between the two channels is due to the spatial overlap of the excited modes and the geometry of the detector segment. The separation of the two input signals at the receive side is simple as will be shown in the next section.

IV. Performance Results

We compare the bit error rate performance of an optical SISO link with a 2×2 and a 4×2 (four receive and 2 transmit elements) optical MIMO link, where we submit two data streams simultaneously over different mode groups (modal multiplexing). We consider in both cases an optical system where the received pulses may overlap, resulting in intersymbol interference (ISI). Note, that the symbol duration T_{s} in the MIMO transmission scheme is doubled and hence, the ISI should be less severe than in the SISO scheme.

A simple suboptimal receiver scheme for the $n \times m$ MIMO channel is depicted in Figure 2. In case of SISO transmission, we have only one branch. The signal $r_i(t)$ at photodetector i is corrupted additively by white Gaussian noise (AWGN), which is due to the electronics after photo-detection. Note, that the choice of AWGN is an approximation that may overestimate the bit error rate [13].

The electrical signal-to-noise ratio SNR_i in branch i is defined as

$$\mathrm{SNR}_i = \frac{\mathrm{E}\left\{\left(\int_0^{T_{\mathrm{s}}} r_i(t)\ \mathrm{d}t\right)^2\right\}}{\mathrm{E}\left\{\left(\int_0^{T_{\mathrm{s}}} n_i(t)\ \mathrm{d}t\right)^2\right\}} = \frac{P_{\mathrm{opt},i}^2}{\sigma_{\mathrm{n}}^2}. \qquad (7)$$

where E denotes the expectation operator and $P_{\mathrm{opt},i}$ the optical energy that photodetector i receives. The T_{s} spaced signal samples $y_i(kT_{\mathrm{s}})$ are obtained by integrating the received power over one symbol period and sampling at the end of the integration. For data detection we consider perfect channel knowledge at the receiver.

SISO Data Detection. We perform symbol-by-symbol processing which is suboptimal in presence of ISI. The decision variable d in time slot k is obtained by

$$d(k) = \int_{kT_{\mathrm{s}}}^{(k+1)T_{\mathrm{s}}} [r(t) + n(t)]\ \mathrm{d}t = m(k) + \epsilon(k), \qquad (8)$$

where $\epsilon(k) \sim N(0, \sigma_n^2)$ and $\sigma_n^2 = \mathrm{E}\left\{\left(\int_{kT_{\mathrm{s}}}^{(k+1)T_{\mathrm{s}}} n(t)\ \mathrm{d}t\right)^2\right\}$ is the same for all k.

When a "one" is transmitted in time slot k, ISI can only increase the received optical energy $m(k)$ in symbol interval $[kT_\mathrm{s}, (k+1)T_\mathrm{s}]$. The smallest received energy and the largest error probability result when a "one" is surrounded by "zeros". In that case the received energy is given by

$$m(k) = m_1 = (1-\delta)M, \tag{9}$$

where $M = \int_{-\infty}^{\infty} r(t)\ \mathrm{d}t$ is the optical energy of the whole receive pulse belonging to one data bit and

$$\delta = 1 - \frac{1}{M}\int_{kT_\mathrm{s}}^{(k+1)T_\mathrm{s}} r(t)\ \mathrm{d}t \tag{10}$$

denotes the relative energy outside the signaling interval $[kT_\mathrm{s}, (k+1)T_\mathrm{s}]$.

When a "zero" is transmitted in time slot k, maximal ISI occurs when the "zero" is surrounded by "ones". The optical energy received in this signaling interval corresponds to

$$m(k) = m_0 = \delta M. \tag{11}$$

For given $m(k)$ the decision variable d in (8) is Gaussian distributed with mean equal to either m_0 or m_1 and variance σ_n^2. The threshold for binary detection in case of equal probable data symbols is determined as $\alpha = (m_0 + m_1)/2$.

MIMO Data Detection. In the case of MIMO transmission the received signals experience multi stream interference (MSI) in addition to ISI. In order to have a fair comparison with the SISO case we apply Maximum Likelihood (ML) vector detection, which mitigates MSI but not the ISI which occurs in the individual data streams. To eliminate ISI one would have to use an ML vector sequence detector. The ML receiver chooses the data vector $\mathbf{a}$ that solves

$$\hat{\mathbf{a}} = \arg\min_{\mathbf{a}} \left\| \mathbf{y} - \int_{kT_\mathrm{s}}^{(k+1)T_\mathrm{s}} \mathbf{r}(t,\mathbf{a})\mathrm{d}t \right\|_2^2, \tag{12}$$

where $\mathbf{r}(t,\mathbf{a})$ contains the signals determined in (4) and $\mathbf{y}$ the noisy receive signals. In Figure 4 we determined bit

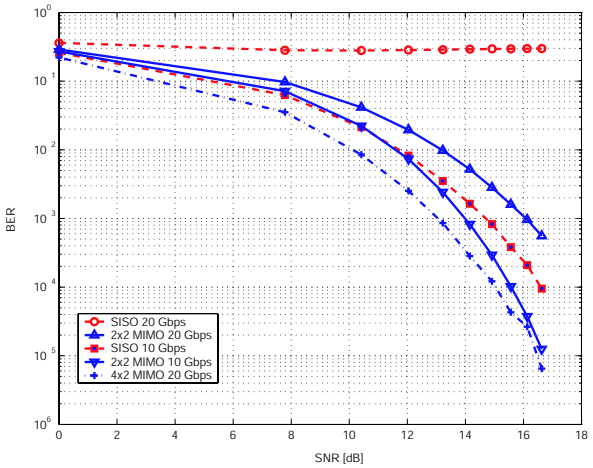

Fig. 4. Bit error rates vs. electrical signal-to-noise ratio for different transmission schemes.

error curves by Monte Carlo simulations for different settings. For the simulation we use the channel described in Section III. We compare 20 Gbps and 10 Gbps SISO links with corresponding 2×2 MIMO links that have the same aggregate data rate. We can see that with the MIMO scheme the bit error rates are improved due to the increased signaling interval and therefore the reduced ISI. The improvement from the 10 Gbps MIMO link to the 10 Gbps SISO link is less due to the fact, that the ISI in the 10 Gbps SISO link is not as large as in the 20 Gbps SISO transmission. Additionally, we simulated a 4×2 MIMO channel which is also depicted in Figure 4. We see that this scheme outperforms the other schemes due to the increased spatial diversity.

V. Conclusions

We have shown that in highly multimodal waveguides optical MIMO transmission schemes outperforms SISO schemes with respect to bit error rates. Due to the doubled signaling interval in a 2×2 and a 4×2 MIMO scheme the intersymbol interference is less severe than in the SISO scheme having the same data rate. This allows either for equalizers with lower per-stream complexity (keeping the data rate constant) or for increasing the data rate by keeping the per-stream equalizer complexity constant.

References

[1] A. Himmler, E. Griese, J. Schrage, T. Bierhoff, A. Wallrabenstein, and M. G., "Modeling of highly multimodal optical interconnects for time domain analysis," in *Digest of 2000 LEOS Summer Topical Meetings, Electronic-Enhanced Optics*, (Aventura/FL (USA)), pp. 43–44, 2000.

[2] J. Moisel, J. Guttmann, H.-P. Huber, O. Krumpholz, M. Rode, R. Bogenberger, and K.-P. Kuhn, "Optical backplanes with integrated polymer waveguides," *Optical Engineering*, vol. 39, no. 3, pp. 673–679, 2000.

[3] C. Argon, M. Patel, S. W. McLaughlin, and S. Ralph, "Exploiting diversity in multimode fiber communications links via multisegment detectors and equalization," *IEEE Communication Letters*, vol. 7, no. 8, pp. 400–402, 2003.

[4] A. Paulraj, R. Nabar, and D. Gore, *Introduction to Space-Time Wireless Communications*. Cambridge, 2003.

[5] M. Jungo, D. Erni, and W. Baechtold, "Segmented VCSEL contact geometry for active coupling efficiency enhancement," in *Workshop on Compound Semiconductor Devices and Integrated Circuits (WOCSDICE'03)*, vol. 5-3, (Fürigen, Switzerland), 2003.

[6] M. Jungo, *Spatiotemporal vertical-cavity surface-emitting laser model for advanced simulations of optical links*, vol. 30 of *Series in Quantum Electronics*. Konstanz: Hartung-Gorre Verlag, 2003.

[7] J. Sutherland, G. George, and J. P. Krusius, "Optical coupling and alignment tolerances in optoelectronic array interface assemblies," in *Proc. of the 45th Elec. Comp. & Tech. Conf.*, pp. 577–583, 1995.

[8] N. Delen and B. Hooker, "Free-space beam propagation between arbitrarily oriented planes based on full diffraction theory: a fast fourier transform approach," *J. Opt. Soc. Am, A*, vol. 15, no. 4, 1998.

[9] E. Marcatili, "Dielectric rectangular waveguide and directional coupler for integrated optics," *The Bell System Technical Journal*, vol. 48, pp. 2071–2103, 1969.

[10] D. Marcuse, *Theory of Dielectric Optical Waveguides*. Quantum Electronics-Principles and Applications, Boston: Academic Press, 2nd ed., 1997.

[11] D. Lenz, B. Rankov, D. Erni, W. Baechtold, and A. Wittneben, "Modal multiplexing in higly overmoded multiple-input multiple-output optical waveguides," *Journal of Lightwave Technology*, in preparation.

[12] G. P. Agrawal, *Fiber-Optic Communication Systems*. Wiley Series in Microwave and Optical Engineering, New York: John Wiley & Sons, 3rd ed., 2002.

[13] D. Marcuse, "Calculation of bit-error probability for a lightwave system with optical amplifiers and post-detection gaussian noise," *Journal of Lightwave Technology*, vol. 9, no. 4, pp. 505–513, 1991.